JOURNAL OF PETROLEUM GEOMECHANICS
(JPG)

Effect of oil-contamination on behavior of geocell-reinforced soil abutment wall

Foad Changizi[1]; Arash Razmkhah[*2]; Hasan Ghasemzadeh[3]; Masoud Amelsakhi[4]

1.Department of Civil Engineering, South Tehran Branch, Islamic Azad University, Tehran, Iran
2.Department of Civil Engineering, South Tehran Branch, Islamic Azad University, Tehran, Iran
3.Civil Engineering Faculty, K. N. Toosi University of Technology, Tehran, Iran
4.Department of Civil Engineering, Qom University of Technology, Qom, Iran

Received:12 March 2022; Accepted: 27 April 2022

DOI: 10.22107/jpg.2022.333533.1161

Keywords

Shear Wave Velocity
ELM
MLP
Machine Learning
Well log data

Abstract

Oil-contaminated soil should be remediated or can be used as filling materials. The evaluation of the bearing capacity of geocell-reinforced soil abutment wall is the purpose of the present study under conditions of the backfill contaminated soil through numerical modeling based on PLAXIS 2D. The behavior of the wall is studied based on changes in the amount of oil, the distance between the strip footing and the wall facing (D), the height (hg), the length (L) values and the number of geocell layers as well as the wall slope. The numerical results showed that the maximum length geocell of the layer required is 2.16 times the footing width and the optimum geocell length is equal to 1.0 times the wall height (H). The increase in the geocell height and number of geocell layers leads to an increase in the soil stiffness, leading to an increase in the bearing capacity of footing and decrease in the horizontal displacement of the wall. The results showed that reducing the slope of the wall is very effective in reducing the horizontal displacement of the wall. In general, the soil contamination due to the oil has a negative effect on wall performance. In other words, an increase in the amount of oil reduces the percentage improvement in the wall behavior due to an increase in the height, length and the number of geocell layers.

1. Introduction

Soil contaminated with oil is one of the most dangerous contaminants which can lead to irreparable damage to the environment. Since the removal of pollution from the soil is costly, the contaminated soil can be used in projects such as the building foundation and the backfill abutment wall (Ghasemzadeh and Tabaiyan, 2017). The oil-contaminated soils have different geomechanical properties compared to non-contaminated soil properties. (Singh et al., 2008; Kermani and Ebadi, 2012; Khosravi et al. 2013). Nasehi et al. (2015) reported that the friction angle of soil decreases by about 25% with mixing 6% of gas oil into the sand. The easy movement of soil particles due to lubrication of oil reduces the friction angle of soil (Al-Adili et al., 2017). Safehian et al. (2018) believed that the soil contamination with 8% diesel results in a 54% reduction in the unconfined compressive strength of the illite soil. Ahmadi et al. (2021) acknowledged that if the percentage of clay in the sand was high, the maximum dry density of sand decreases with an increase in the amount of oil. By changing in the geotechnical parameters due to the presence of the oil, the design parameters of the footing will be changed. Nasr (2015) evaluated the bearing capacity of footing of oil-contaminated sand. The results showed that increasing the depth of contamination leads to reduction in the bearing capacity of footing.

* Iran, Tehran, Islamic Azad University, South Tehran Branch, Department of Civil Engineering, Tl: 09121447223, Email: a_razmkhah@azad.ac.ir

Fadhil Al-Adly et al. (2019) acknowledged that the contaminated sand with 10% oil reduces the bearing capacity of the foundation by up to 69%. The oil contamination of soil decreases the ultimate lateral capacity of the soil (Abdelhalim et al., 2020). In research conducted by Alfach and Wilkinson (2020), Oil contamination has a negative effect on the geotechnical behavior of a bridge piles foundation, which is reflected by the displacement of the soil. Therefore, it can be said that the oil changes the geomechanical parameters of the soil that must be considered in the designs.

The good performance of geocells in the improvement of mechanical properties of soil has led to their use in various civil engineering projects. Therefore, the various studies have been conducted to evaluate the effect of geocells on the behavior of foundations (Thallak et al., 2007; Madhavi Latha and Somwanshi, 2009; Dash, 2012; MoghaddasTafreshi et al., 2016; Venkateswarlu et al., 2018), railways (Yang et al., 2012; Moghaddas Tafreshi et al., 2014; Pokharel et al., 2018; Inti and Tandon, 2021) and retaining wall structures (Ling et al., 2009; Leshchinsky et al., 2009; Soudé et al., 2013; Chen et al., 2013). Due to the cellular structure of the geocell, the soil particles are surrounded within the geocell layer, leading to an increase in the shear strength of the soil (Moghaddas Tafreshi and Dawson, 2010). The positive effect of geocell on the bearing capacity of the soil depends on the amount of relative density so that the increase in bearing capacity due to the geocell is more visible for relative densities above 70% (Dash, 2010). Zhou and Wen (2008) believed that the geocell layer significantly increases the subgrade reaction coefficient. With increasing the elastic modulus of geocell materials, the rate of increase in bearing capacity of soil reinforced with geocell increases (Pokharel et al., 2010). In general, it can be said that the geometrical properties of the geocell layer play an important role in the behavior of geocell-reinforced soil. Many researchers have studied the application of geosynthetics in retaining walls (Skinner and Rowe, 2005; Tatsuoka et al., 2016; Xiao et al., 2016; Li et al., 2020). The use of geocell in the retaining wall has been noticed by researchers. Chen and Chiu (2008) showed that using reinforcement in the gravity wall made with geocell can improve the behavior of the wall. Xie et al. (2009) studied the behavior of the geocell-gravity wall. The results showed that the performance of this type of wall depends on the wall width. Based on a study conducted by Song et al. (2014), the increase in the ratio of geocell length to wall height leads to decrease in the horizontal displacement of gravity walls made with geocell. Madhavi Latha and Manju (2016) by physically modeling of the geocell-gravity wall under seismic loading showed that the maximum horizontal displacement of the wall occurs at top of the wall. Song et al. (2018a) evaluated the failure wedges of the geocell-gravity wall. The results showed that the sliding soil wedges become larger with an increase in the loading location. The previous research studies have evaluated the application of geocell in gravity walls, in which the use of geocell in the abutment wall as reinforcement has rarely been evaluated. In general, in previous research studies, the geocell has been mostly used for wall facing, but rarely as reinforcement.

Various researches have been evaluated the geocell performance by numerical method. However, due to the cellular structure of the geocell, the numerical modeling of the geocell layer is not easy. In one method of numerical modeling of geocell, the geocell layer filled with soil is considered as a composite soil layer with modified strength parameters (Madhavi Latha and Somwanshi, 2009; Hegde and Sitharam, 2013; Mehdipour et al., 2013). Hegde and Sitharam (2015) modeled soil reinforced with a geocell layer by fast Lagrangian analysis of continua in 3D (FLAC3D), and the effect of the size of the geocell pocket opening was examined as a variable parameter in the bearing capacity was examined. Biabani et al. (2016) conducted a

numerical study on geocell-reinforced soil with ABAQUS, and the tensile stress distributed non-uniformly on the geocell. Song et al. (2018b) studied the effects of the apparent cohesion on the behavior of the geocell-gravity wall by the Finite Element code ABAQUS. They found that for soils with internal friction angle of less than 35°, the resistance reduction technique is appropriate to evaluate the wall stability. In previous research studies, the numerical modeling of geocell has been done for soil reinforced with a geocell layer. Also, in the context of the retaining wall, the geocell layer has played the role of the wall facing, and has not been done the numerical modeling of the abutment wall reinforced with geocell.

In this study, the behavior of abutment wall reinforced with geocell under conditions with and without oil pollution is evaluated by a two-dimensional finite element modeling based on PLAXIS 2D. In order to verify the numerical modeling, the results of the numerical model are compared with the results obtained from the laboratory model performed by Changizi et al. (2022). Then, the wall behavior is evaluated by changing the parameters such as height, length and the number of geocell layers, wall facing slope and the horizontal distance of the foundation from the wall. In the next step, the behavior of the wall with oil- contaminated backfill sand is evaluated and compared with the case of geocell layers with non-contaminated soil.

2. Numerical Modeling

PLAXIS 2D as a finite element program was used for the numerical modeling of geocell-reinforced soil abutment wall in the plane-strain condition. To verify the numerical model, the dimensions of the simulated wall are equal to the dimensions of the physical model made by Changizi et al. (2022). In fact, the wall length of the numerical model is 1.6 m and the wall height is 0.8 m. The constant parameters are included the foundation width (B), the depth of the first geocell layer (u) and the wall height (H), which are equal to 15 cm, 1.5 cm and 80 cm, respectively. Also, the variable parameters are included the amount of oil height, length and number of geocell layers, wall facing slope and the horizontal distance of the foundation from the wall. The amount of oil is considered equal to 3%, 6%, 9% and 12%. The height of the geocell layers (hg) as a variable parameter have has become dimensionless with foundation width, and the hg/B ratio has been considered equal to 0.3, 0.4, 0.5, 0.6 and 0.7. The length of the geocell (L) is dimensionless with the height of the wall and the L/H ratio varies in the range of 0.7, 1.0 and 1.5. Also, the number of geocell layers (N) is equal to 6, 8 and 10. The horizontal distance between the foundation and the wall is dimensionless with the wall height (D/H), and the D/H ratio varies in the range of 0.2, 0.35 and 0.5. The wall slope (α) is considered to be variable and equal to 90°, 80° and 70°. The bearing capacity of foundation and the horizontal displacement of wall are evaluated by changes in the variable parameters. The set of numerical models performed in this study is listed in Table 1.

1. Test material

The behavior of backfill soil was simulated with the Mohr-Coulomb model. The Mohr-Coulomb model is an elastic-plastic criterion and the most common model for showing the shear failures in the soil. Because the failure in the abutment wall model occurs on a plane with critical combination of the normal and shear stress, the Mohr-Coulomb model can well determine this plane. The Mohr-Coulomb model is widely used by designers in the geotechnical analysis due to its simplicity and tangible parameters in the geotechnical topics. The mathematical relation of Mohr-Coulomb criterion is in the form of Eq. (1):

$$\tau=\sigma\tan(\varphi)+c \quad (1)$$

where τ = the shear stress, σ = the normal stress, φ = the internal friction angle of soil and c = the cohesion of the soil. Based on the relations in the Mohr circle:

$$\sigma=\sigma\_m-\tau\_m \sin\varphi \quad (2)$$

$$\tau=\tau\_m \cos\varphi \quad (3)$$

$\tau_m=(\sigma_1-\sigma_3)/2$ (4)
$\sigma_m=(\sigma_1+\sigma_3)/2$ (5)

where σ_1 = the maximum main stress and σ_3 = the minimum main stress.

Table 1. Numerical tests of geocell-reinforced soil wall

Test	*N*	*Oil content (%)*	*D/H*	*L/H*	h_g/B	*α (degree)*
1	*6*	-	*0.2*	*0.7*	*0.3*	*90*
2	*6*	-	*0.35*	*0.7*	*0.3*	*90*
3	*6*	-	*0.5*	*0.7*	*0.3*	*90*
4	*6*	-	*0.2*	*1.0*	*0.3*	*90*
5	*6*	-	*0.35*	*1.0*	*0.3*	*90*
6	*6*	-	*0.5*	*1.0*	*0.3*	*90*
7	*6*	-	*0.2*	*1.5*	*0.3*	*90*
8	*6*	-	*0.35*	*1.5*	*0.3*	*90*
9	*6*	-	*0.5*	*1.5*	*0.3*	*90*
10	*6*	*3*	*0.35*	*1.0*	*0.3*	*90*
11	*6*	*6*	*0.35*	*1.0*	*0.3*	*90*
12	*6*	*9*	*0.35*	*1.0*	*0.3*	*90*
13	*6*	*12*	*0.35*	*1.0*	*0.3*	*90*
14	*6*	-	*0.35*	*1.0*	*0.4*	*90*
15	*6*	-	*0.35*	*1.0*	*0.5*	*90*
16	*6*	-	*0.35*	*1.0*	*0.6*	*90*
17	*6*	-	*0.35*	*1.0*	*0.7*	*90*
18	*6*	*3*	*0.35*	*1.0*	*0.6*	*90*
19	*6*	*6*	*0.35*	*1.0*	*0.6*	*90*
20	*6*	*9*	*0.35*	*1.0*	*0.6*	*90*
21	*6*	*12*	*0.35*	*1.0*	*0.6*	*90*
22	*8*	-	*0.35*	*1.0*	*0.3*	*90*
23	*10*	-	*0.35*	*1.0*	*0.3*	*90*
24	*8*	*3*	*0.35*	*1.0*	*0.3*	*90*
25	*8*	*6*	*0.35*	*1.0*	*0.3*	*90*
26	*8*	*9*	*0.35*	*1.0*	*0.3*	*90*
27	*8*	*12*	*0.35*	*1.0*	*0.3*	*90*
28	*6*	-	*0.2*	*1.0*	*0.3*	*80*
29	*6*	-	*0.2*	*1.0*	*0.3*	*70*
30	*6*	-	*0.35*	*1.0*	*0.3*	*80*
31	*6*	-	*0.35*	*1.0*	*0.3*	*70*
32	*6*	-	*0.5*	*1.0*	*0.3*	*80*
33	*6*	-	*0.5*	*1.0*	*0.3*	*70*
34	*6*	*3*	*0.35*	*1.0*	*0.3*	*70*
35	*6*	*6*	*0.35*	*1.0*	*0.3*	*70*
36	*6*	*9*	*0.35*	*1.0*	*0.3*	*70*
37	*6*	*12*	*0.35*	*1.0*	*0.3*	*70*

The mechanical properties of the modeled sand are listed in Table 2. The abutment wall is modeled on a dense layer of sand with the Mohr Coulomb behavioral model, which the characteristics are shown in Table 2. The wall facing is modeled with prefabricated concrete blocks in dimensions of 0.1, 0.1 and 0.05 m for height, width and thickness, respectively. The behavioral model of the blocks of wall facing was considered the linear-elastic. The mechanical properties of the blocks of wall facing are also presented in Table 2.

Table 2. Mechanical properties of the backfill soil

Soil	*Model type*	*Unit weight (kN/m³)*	*Poisson coefficient*	*Cohesion (kPa)*	*Angle of friction (degree)*	*Angle of dilatation (degree)*	*Young's module (kPa)*
Backfill sand	*Mohr Coulomb*	*15*	*0.3*	*1*	*34*	*4*	1.5×10^4
Dense sand	*Mohr Coulomb*	*18*	*0.3*	*1*	*34*	*4*	1.8×10^4
blocks of wall facing	*linear-elastic*	*24*	*0.25*	*70*	*54*	*0*	9×10^4

In this research, the geocell has been used as reinforcement. However, due to the cellular structure of the geocell, the geocell cannot be modeled in two-dimensional conditions. Therefore, the equivalent composite technique has been used for the numerical modeling of geocell layers. In other words, the sand-filled geocell layer is considered as a soil layer with modified strength. The angle of friction and the unit weight of equivalent composite is the same as the angle of friction and the unit weight of backfill soil (Bathurst and Karpurapu, 1993; Rajagopal et al., 1999). But, because of the confinement due to geocell the cohesion of equivalent composite is greater than that of backfill soil (Madhavi Latha and Rajagopal, 2007). According to the result reported by Madhavi Latha and Rajagopal (2007), the cohesion due to geocell (cr) can be calculated from Eq: (6).

$$c_r = \frac{\Delta\sigma_3}{2}\sqrt{k_p} \tag{6}$$

where kp is the coefficient of passive earth pressure and Δσ3 is the additional confining pressure due to the membrane stresses. Δσ3 can be calculated from Eq. (7):

$$\Delta\sigma_3 = \frac{2M}{d_g}\left(\frac{1-\sqrt{1-\varepsilon_a}}{1-\varepsilon_a}\right) \tag{7}$$

where dg is the diameter of the equivalent circular area of the pocket size of the geocell and M is the tensile stiffness of the geocell material at an axial strain of ε_a. According to the geocell layer used in the study by Changizi et al. (2022), the dg is 0.05 m and for the axial strain of 5%, the tensile stiffness (M) was calculated equal to 50 kN/m. Therefore, based on Eq. (6) and (7), the amount of cohesion due to the geocell is equal to 49 kPa. Madhavi Latha (2000) reported Eq. (8) to calculate the elastic modulus of the sand-filled geocell layer (Eg):

$$E_g = 4(\Delta\sigma_3)^{0.7}(k_u + 200M^{0.16}) \tag{8}$$

where Ku is the dimensionless modulus parameter of the unreinforced sand. At Ku = 240, the value of the elastic modulus of the equivalent composite (Eg) is calculated to be 38000 kPa.

In previous studies, the equivalent composite technique was used for horizontal ground, and the use of the tensile capacity of a sand-filled geocell layer was not significant. However, in the numerical model of the abutment wall, the equivalent composite must be able to withstand tensile stresses. For this aim, a layer of geogrid that was used to make the geocell is placed in the middle of the equivalent composite and attached to the block of wall facing. For this purpose, the geogrid element has been used and the tensile stiffness (EA) equal to 50 kN/m has been considered. The geogrid specification used in the numerical model (Table 3) was similar to the geogrid used in the laboratory model performed by Changizi et al. (2022).

Table 3 physical properties of geogrid (Changizi et al., 2022)

Parameter	*MD*	*XMD*
Aperture size (mm)	*3.5*	*1.5*
Thickness (mm)	*0.5*	*0.5*
Peak tensile strength (kN/m)	*3.03*	*1.34*
Tensile strength at 2% strain (kN/m)	*1.1*	*0.3*

Note: MD stands for machine direction; XMD stands for cross-machine direction

As shown in previous research, the geomechanical characteristics of oil-contaminated soil are different from those of clean soil. According to the defined behavioral model, the soil parameters important in this study include the cohesion and the internal friction angle of sand. Since the cohesion of sand is almost zero, the oil contamination into the clean sand can be ignored due to the negligible effect on the soil cohesion. Nasr (2009) reported a similar result. Therefore, the cohesion of oil-contaminated sand is considered equal to the cohesion of clean sand. Based on previous research studies, the range of reduction in the internal friction angle of sand contaminated with 3%, 6%, 9% and 12% oil was equal to 32°, 30°, 28.5° and 27.5°, respectively (Soltani-Jigheh et al., 2018; Nasser, 2009). Based on the research conducted by Soltani-Jigheh et al. (2018), the properties of oil for the parameters such as viscosity, the density (at 25◦C), American Petroleum Institute (API) gravity (at 60◦F), flash point (◦C) and specific gravity (at 25◦C) are equal to 41.2 g/ms, 0.895 g/cm3, 26.8, 44.2 and 0.89, respectively. Fig. 1 represents a finite-element model of abutment wall reinforced with 6 geocell layers.

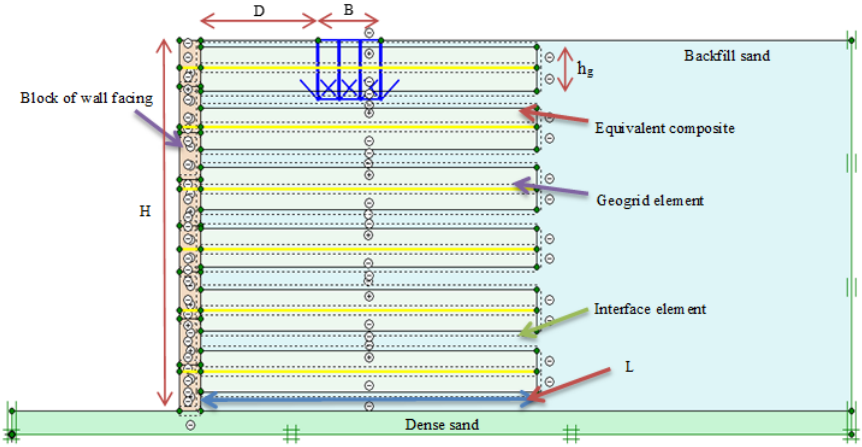

Fig. 1. Elements of the model including backfill soil, equivalent composite, geogrid, interface and block of wall facing

2. Interface properties and boundary conditions

The interface element is used to define the interaction between the wall facing and the backfill soil, the interaction of the equivalent composite and the backfill soil as well as the geogrid and the equivalent composite. Since the interface friction angle between the wall facing and backfill soil is considered to be 2/3 of the internal friction angle of the backfill soil, the resistance reduction factor (Rinter) is considered to be 0.66. However, the interface between the equivalent composite and the backfill soil as well as the geogrid and the

equivalent composite was defined as a fully bonded interface (Rinter = 1.0). The boundary conditions for displacements were considered the same for all models. The bottom of the model is fixed so that the base of the model does not have horizontal and vertical displacements. In addition, the vertical boundary of the model towards the backfill soil is restricted in the horizontal direction and free to move in the vertical direction.

3. Mesh

The physical model by Changizi et al. (2022) is numerically simulated and the meshed model is depicted in Fig. 2. The numerical model was meshed based on fifteen nodded triangular elements. To increase in the accuracy of estimating stresses and displacements in the numerical models, the fine meshing has been used. The loading is applied in the form of displacement control so that the displacement increases uniformly until the maximum defined value is reached.

4. Verification of numerical model

The numerical model has been verified with the results of the physical model obtained from the research of Changizi et al. (2022) for a wall reinforced with 6 layers of geocell. The bearing capacity of footing and the horizontal displacement of the wall for the numerical model have been compared with these of the laboratory model. Fig. 3 draws the comparison between the pressure-settlement curves of the numerical model and the laboratory model at L/H = 0.7 for different the D/H ratios. According to Fig. 3, the results obtained from the numerical model are in good agreement with the laboratory results. From Fig. 3 it can be seen that with increase in the D/H ratio, the difference results between numerical simulation results and the laboratory results decreases.

The comparison between the maximum horizontal displacement of the wall in the numerical model and that of the wall in the laboratory model is shown in Fig. 4. It shows the fact that the numerical model can well estimate the maximum horizontal displacement of the wall. The maximum horizontal displacement of the wall in Fig. 5 has occurred at the z/H = 0.625 (z = height from the bottom of the wall) for all ratios s/B and ratio D/H, and this is in good agreement with the laboratory results. As shown in Figure 4, the horizontal displacement of the wall is linearly related to the vertical displacement of the foundation. In other words, the changes in the horizontal displacement of the wall depend more on the vertical displacement of the foundation than other variable parameters.

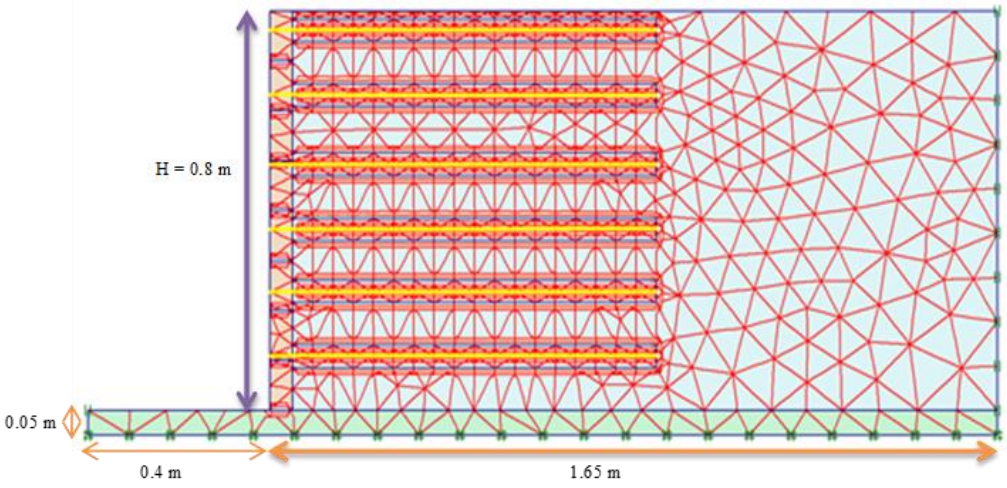

Fig. 2. Numerical model test with the generated mesh and boundary condition

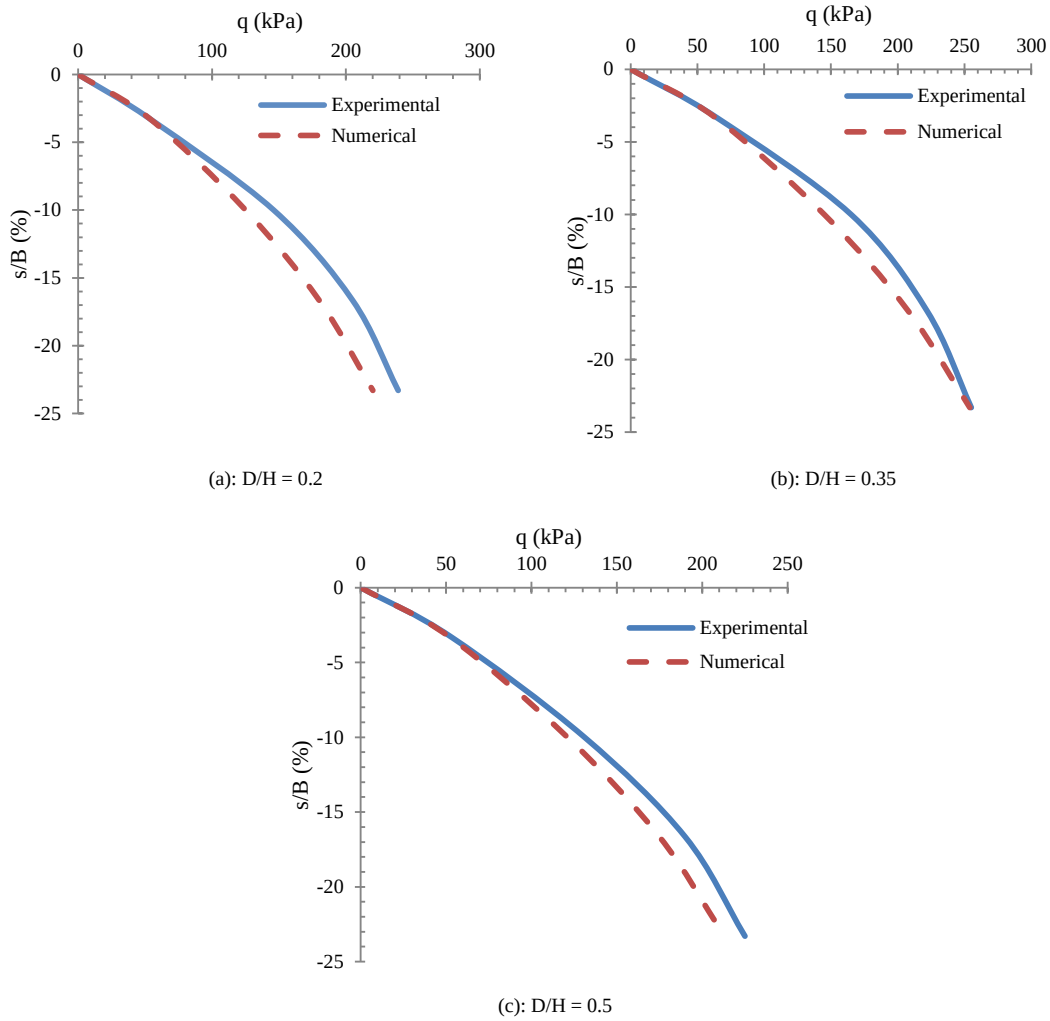

Fig. 3. Comparison of the bearing capacity of footing between the numerical model results and the experimental results by Changizi et al. (2022) for L/H = 0.7: (a) D/H = 0.2, (b) D/H = 0.35, (c) D/H = 0.5

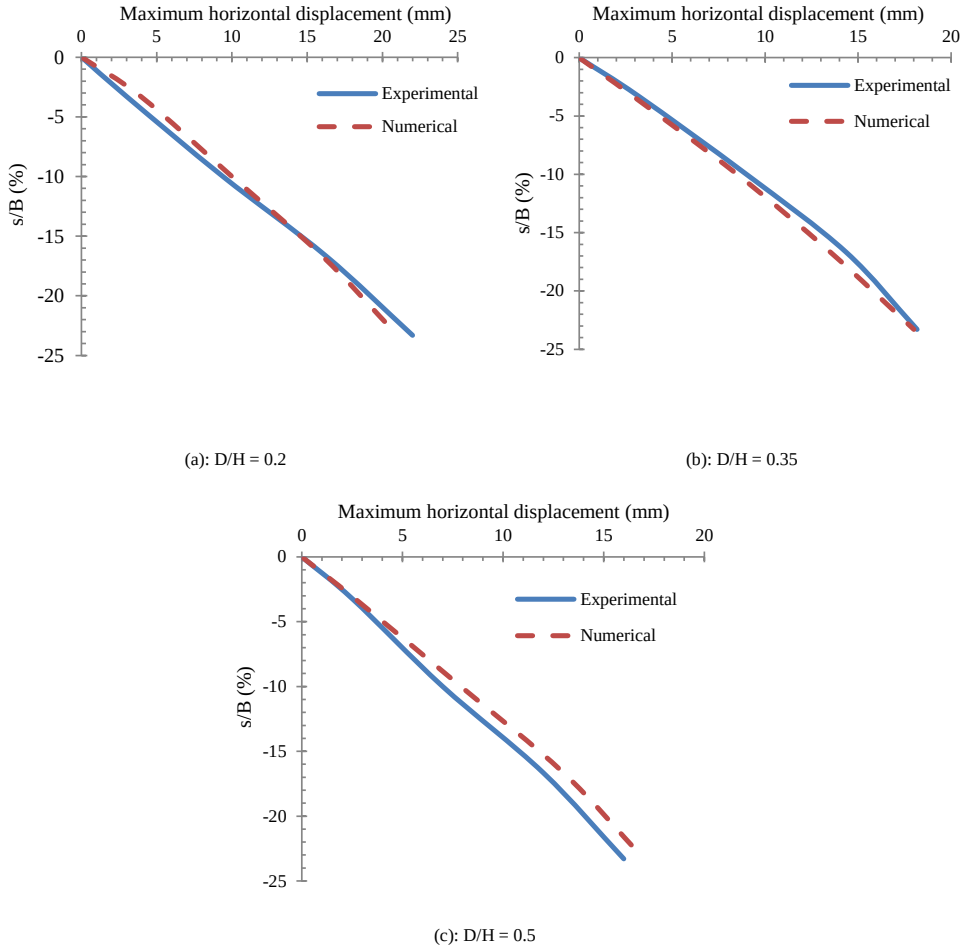

Fig. 4. Comparison of the maximum horizontal displacement of wall between the numerical model results and the experimental results by Changizi et al. (2022) for L/H = 0.7: (a) D/H = 0.2, (b) D/H = 0.35, (c) D/H = 0.5

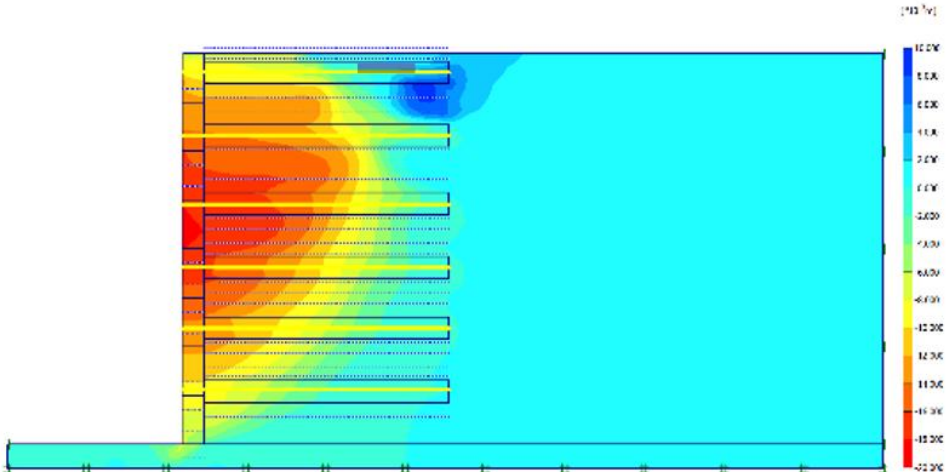

Fig. 5. Contour horizontal displacement of the wall

5. Results

5.1 Effect of L/H ratio and D/H ratio

The change in the geocell length and the horizontal distance of footing from the wall facing leads to change in the footing performance. Fig. 6 shows the bearing capacity of footing for the various settlements to foundation width ratio (s/B) at different the D/H ratio and the L/H ratio. It can be seen from Fig. 6 that increase in the geocell length has a positive effect on the bearing capacity. According to Fig. 6, an increase in the D/H ratio leads to increase in the bearing capacity of footing. However, at L/H = 0.7, when the D/H ratio increases from 0.35 to 0.5, the bearing capacity decreases. The reason for this phenomenon is that in D/H = 0.5, the foundation is placed at the end of the geocell layer, which causes the asymmetric settlement of footing, resulting in reduction in the bearing capacity. By examining Fig. 6, it can be realized that the effectiveness of the geocell length on the bearing capacity depends on the amount of D/H ratio. For example, at the D/H = 0.5 and s/B = 10%, with increasing the L/H from 0.7 to 1.0, the bearing capacity of footing increases by about 40%. However, at the D/H = 0.2 and s/B = 10%, with increasing the L/H from 0.7 to 1.0, the bearing capacity of footing increases by about 6%. As a result, it can be declared that the optimum length of geocell layer to achieve the maximum bearing capacity of footing is 2.16 times the footing width from the footing center to the sides.

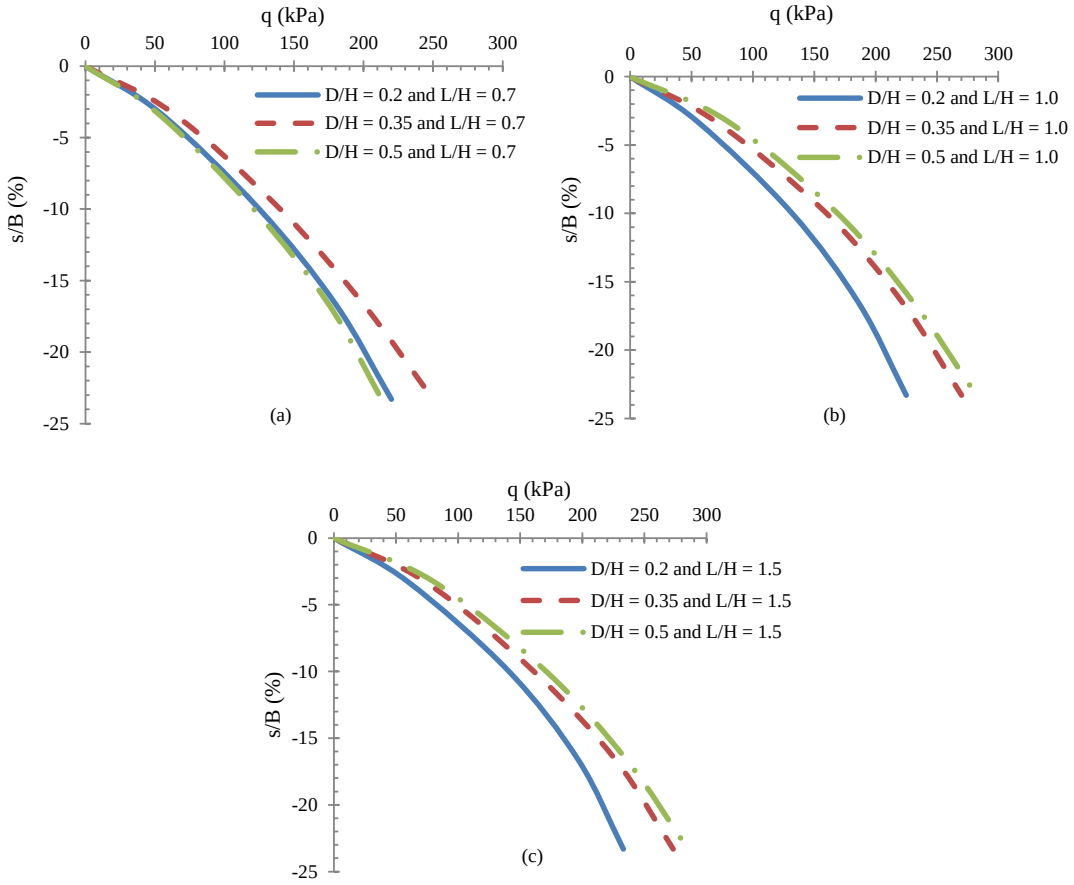

Fig. 6. Bearing capacity (q) - settlement ratio (s/B) curves of the footing on reinforced soil wall for different D/H ratios: (a) L/H = 0.7, (b) L/H = 1.0, (c) L/H = 1.5

The horizontal displacement of wall facing changes with change in the D/H and L/H ratios. The results showed that the maximum horizontal displacement of the wall (ΔHmax) occurs at z/H = 0.625. Table 4 shows the maximum horizontal displacement of the wall facing at different L/H and D/H ratios for various footing pressure. It can be seen from Table 4 that the horizontal displacement of the wall decreases with an increase in the D/H ratio. Indeed, with increasing the D/H ratio, the horizontal stresses due to loading decreases, leading to a reduction in the horizontal displacement of the wall. At L/H = 1.0, with an increase in the D/H ratio from 0.2 to 0.5, the maximum horizontal displacement of the wall is reduced by an average of 37% for different footing pressure. Although ΔHmax decreased with an increase in the D/H ratio, but, ΔH_{max} for L/H = 0.7 and at D/H = 0.5 was greater than that at D/H = 0.35. This can be attributed to the fact that the horizontal displacement curves have been plotted in terms of pressure, on the other hand, the bearing capacity of soil at D/H = 0.5 is less than that at D/H = 0.35, as a result, the ΔHmax at the ratio D/H = 0.5 was more than that at the ratio D/H = 0.35. The increase in the geocell length leads to an increase in the frictional resistance, leading to a decrease in the horizontal displacement of wall. Table 4 shows that increasing the geocell length more than the optimal geocell length (2.16 times the footing width from the footing center) has a negligible effect on the horizontal displacement of the wall.

Table 4 Maximum horizontal displacement of the wall facing at different L/H ratio and D/H ratios

L/H	*D/H*	*Maximum horizontal displacement (mm)*				
		q(kPa)				
		50	*100*	*150*	*200*	*250*
	0.2	*3*	*9*	*14*	*21*	-
0.7	*0.35*	*2.5*	*6*	*10*	*15*	*20*
	0.5	*2.3*	*6.2*	*11*	*17*	-
	0.2	*2.8*	*8.5*	*13*	*19*	-
1.0	*0.35*	*2.3*	*5.5*	*9.5*	*14*	*19*
	0.5	*1.7*	*5*	*9*	*12*	*17*
	0.2	*2.7*	*8.3*	*12*	*18*	-
1.5	*0.35*	*2.2*	*5*	*9.2*	*14*	*18*
	0.5	*1.5*	*4*	*7.3*	*11*	*16*

5.2 Effect of oil content for D/H = 0.35 and L/H = 1.0

According to the results, the D/H = 0.35 and L/H = 1.0 ratios are considered as the optimal condition, and the effect of contamination due to the oil on the bearing capacity has been investigated under noted conditions mentioned. The negative effect of oil on the bearing capacity of footing located on the contaminated backfill soil is shown in Fig.7. Based on Fig. 7, at s/B = 10%, the bearing capacity of footing decreases by 21%, 37.5%, 44% and 47% for backfill soil contaminated with 3%, 6%, 9% and 12% oil contents, respectively. The sliding of particles due to lubrication results in a reduction in the soil stiffness, resulting in a decrease in the bearing capacity of footing. The maximum horizontal displacement of the wall affected by the amount of oil pollution is listed in Table 5. As shown in the Table 5, the horizontal displacement of the wall increases with an increase in the amount of oil, so that with an increase in the amount of oil from 0 to 9%, the maximum horizontal displacement of the wall increases by 78%, 100% and 100% for footing pressure of 50 kPa, 100 kPa and 150 kPa, respectively.

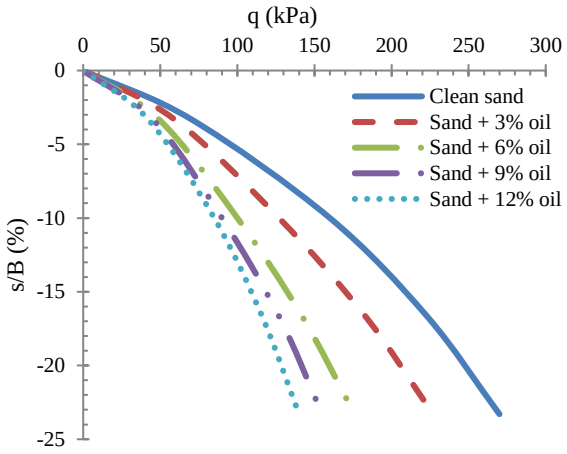

Fig. 7. Bearing capacity (q) - settlement ratio (s/B) curves of the footing on the contaminated backfill soil at D/H =0.35, L/H = 1.0

Table 5 Maximum horizontal displacement of the wall facing at L/H = 1.0 and D/H =0.35 for different amount of oil at various footing pressure

Maximum horizontal displacement (mm)					
	Percentage of oil				
Footing pressure (kPa)	*0*	*3*	*6*	*9*	*12*
50	*2.3*	*2.76*	*3.5*	*4.1*	*4.5*
100	*5.5*	*7.3*	*9.5*	*11*	*12*
150	*9.5*	*12*	*16*	*19*	*20*
200	*14*	*18*	*21*	-	-

5.3 Effect of geocell height

The geocell height (hg) is one of the parameters affecting the geocell performance. Fig. 8 shows the bearing capacity- settlement curves of footing adjacent to the wall for different heights of the geocell layer at D/H = 0.35 and L/H = 1.0. In this part, the geocell height is dimensionless relative to the footing width. Fig. 8 shows that the increase in the hg/B ratio leads to an increase in the bearing capacity of footing. At s/B = 10%, with increasing the hg/B ratio from 0.3 to 0.4, 0.5, 0.6 and 0.7, the bearing capacity of footing increases by 33%, 71%, 114% and 144%, respectively. With an increase in the geocell height, the enclosing effect of the geocell increases, leading to an increase in the stiffness of the geocell layer filled with sand. Eventually, as the stiffness of the backfill soil increases, the bearing capacity of the footing increases. According to Fig. 8, the trend of increasing bearing capacity of footing due to the increase in geocell height after the hg/B = 0.6 decreases. For this reason, it can be stated that the optimal value of the hg/B is 0.6.

The trend of change in the maximum horizontal displacement of the wall due to the change in the hg/B ratio is shown in Fig. 9. It shows the fact that the increase in hg/B ratio has a significant effect on reducing the horizontal displacement of the wall. For example at q = 150 kPa, with increasing the hg/B ratio from 0.3 to 0.4, 0.5, 0.6 and 0.7, the maximum horizontal displacement of the wall decreases by 35%, 57%, 72% and 79%, respectively. From these results it can be seen that the optimal value of the hg/B ratio for reducing the horizontal displacement of the wall is 0.6.

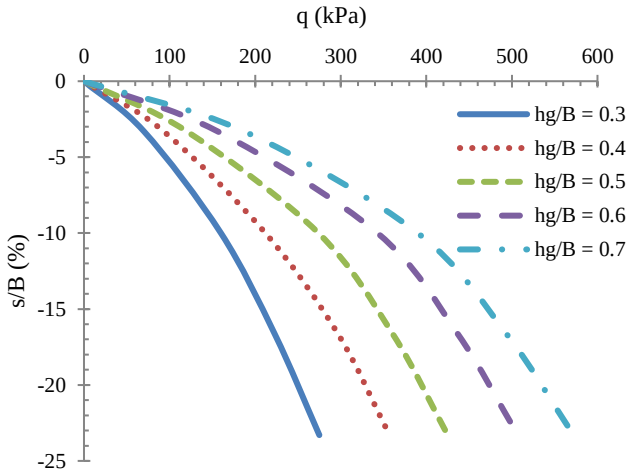

Fig. 8. Bearing capacity (q) - settlement ratio (s/B) curves of the footing on reinforced soil wall for different h_g/B ratios

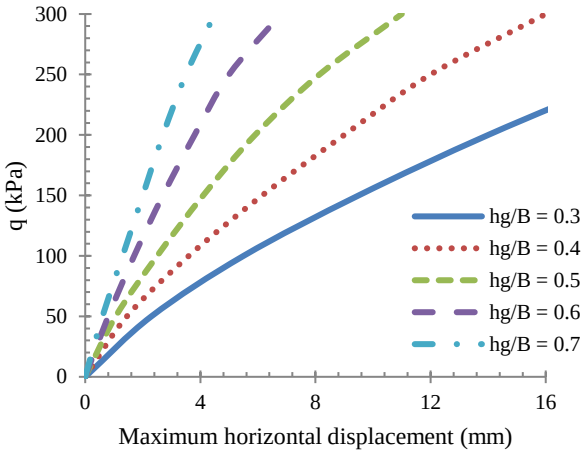

Fig. 9. Maximum horizontal displacement of the wall for different h_g/B ratios

5.4 Effect of oil content for hg/B = 0.6

Although increasing the geocell height leads to an increase in the bearing capacity of footing, but, the soil contamination due to oil contamination decreases the trend of increasing bearing capacity of footing. Fig. 10 shows the negative effect of oil on the bearing capacity of footing at hg/B = 0.6. From Fig. 10 it can be inferred that the largest reduction in the bearing capacity of footing occurs for 6% of oil, so that in this percentage of oil, the bearing capacity of footing decreases by 30%. Needless to say, by increasing the amount of oil by more than 6%, the bearing capacity of footing decreases, but the decreasing trend of bearing capacity of footing decreases. The effect of the oil contamination on the maximum horizontal displacement of wall at the hg/B = 0.6 is shown in Table 6. It expresses the fact that with an increase in the amount of oil up to 6%, the maximum horizontal displacement of the wall increases by 47%. The decrease in the friction between soil particles due to oil is the cause of this phenomenon.

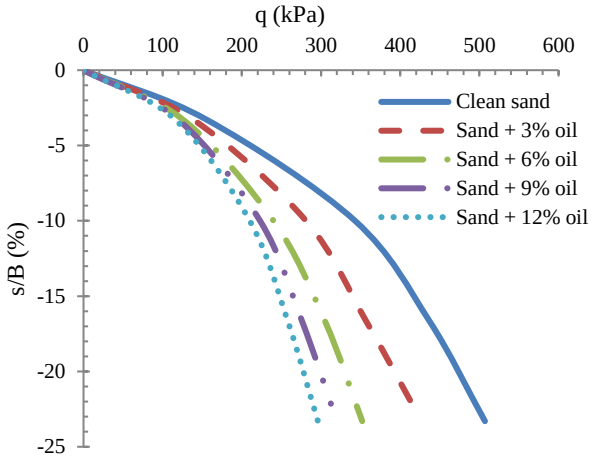

Fig. 10. Bearing capacity (q) - settlement ratio (s/B) curves of the footing at $h_g/B = 0.6$ for different percentages of oil pollution

Table 6 Maximum horizontal displacement of the wall facing at $h_g/B = 0.6$ for different amounts of oil various footing pressure

Maximum horizontal displacement (mm)					
	Percentage of oil				
Footing pressure (kPa)	*0*	*3*	*6*	*9*	*12*
50	*0.8*	*0.86*	*1*	*1.08*	*1.1*
100	*1.7*	*1.92*	*2.2*	*2.4*	*2.5*
150	*2.7*	*3.1*	*3.6*	*4*	*4.3*
200	*3.8*	*4.4*	*5.6*	*6.7*	*7.65*
250	*5*	*6.6*	*9.3*	*11*	*13*
300	*6.8*	*9.8*	*14*	*17*	*19*

7.5 Effect of number of geocell layer

The results showed that the increase in the number of geocell layers improves the bearing capacity of footing (Fig. 11). At s/B = 10%, with increasing the number of geocell layers from 6 to 8 and 10, the bearing capacity of footing increases by 46% and 83%, respectively. An increase in the number of layers means an increase in soil stiffness, leading to an increase in the bearing capacity of the footing. Since the trend of increasing the bearing capacity of foundation decreases after 8 geocell layers, it can be declared that the optimal number of geocell layers is equal to 8.

Fig. 12 shows the maximum horizontal displacement of the wall for different number of geocell layers. As can be seen in Fig. 12, an increase in the number of layers significantly reduces the horizontal displacement of the wall. When the number of geocell layers increases from 6 to 8, the maximum horizontal displacement of wall decreases by 43%, 45%, 47%, 50% and 51% for footing pressure 50 kPa, 100 kPa, 150 kPa, 200 kPa and 250 kPa, respectively. The increase in the footing pressure leads to an increase in the trend of displacement reduction of the wall. The reason for this refers to the fact that as the foundation pressure increases, the frictional resistance between the soil and the geocell layers increases, resulting in the pull outing of geocell being more difficult.

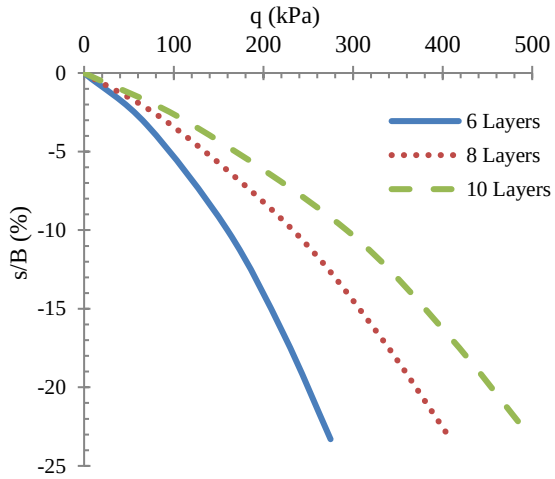

Fig. 11. Bearing capacity (q) - settlement ratio (s/B) curves of the footing on reinforced soil wall for different number of geocell layers

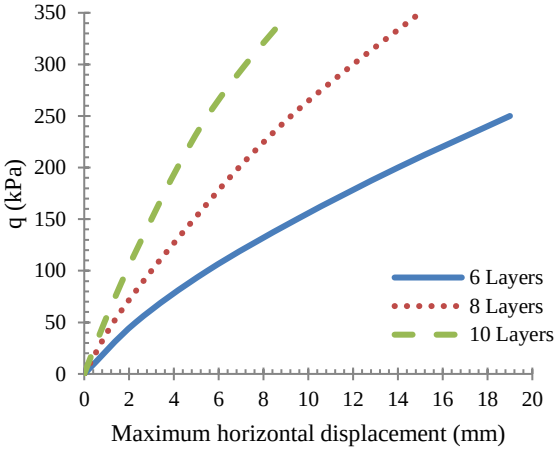

Fig. 12. Maximum horizontal displacement of wall for different number of geocell layer

5.6 Effect of oil content for 8 layers of geocell

Table 7 shows the bearing capacity of footing located on the wall reinforced with 8 geocell layers for different oil contents. As it can be seen Table 7 the oil contamination has reduced the bearing capacity. However, with comparison the results of Table 7 with the results of Fig. 6, it can be said that increasing the number of geocell layers reduces the negative effect of the oil contamination. For example, at 6% of oil, with an increase in the number of geocell layers from 6 to 8, the amount of reduction in the bearing capacity of footing is reduced from 36% to 30%. An increase in the maximum horizontal displacement of the wall due to oil contamination can be seen in Table 8. At footing pressure equal to 200 kPa, the maximum horizontal displacement of the wall with backfill contaminated with 6% oil increases by 59%.

Table 7 Bearing capacity of footing (q) for wall reinforced with 8 layers of geocell for different amounts of oil

Bearing capacity (kPa)					
s/B (%)	*Percentage of oil*				
	0	*3*	*6*	*9*	*12*
3.3	*97*	*81*	*68*	*67*	*64*
10	*233*	*290*	*165*	*149*	*140*
16.6	*329*	*268*	*228*	*205*	*192*
23.3	*409*	*342*	*277*	*250*	*230*

Table 8 Maximum horizontal displacement of wall reinforced with 8 layers of geocell for different amount of oil

Maximum horizontal displacement (mm)					
	Percentage of oil				
Footing pressure (kPa)	*0*	*3*	*6*	*9*	*12*
50	*1.3*	*1.65*	*1.9*	*2.1*	*2.23*
100	*3*	*3.9*	*4.64*	*5.15*	*5.4*
150	*4.9*	*6.2*	*7.55*	*8.4*	*9*
200	*6.9*	*9.3*	*11*	*12*	*13*
250	*9.2*	*12.6*	*15*	*17*	-

5.7 Effect of wall slope

The reduction in the slope of the wall is one of the ways to improve the performance of the wall. The changes in the bearing capacity of the foundation at different slopes of the wall are shown in Fig. 13. The results show that for all D/H ratios, the decrease in the slope of wall leads to increase in the bearing capacity of footing. On average, by reducing the slope of the wall from 90° to 70°, the amount of increase in bearing capacity of footing was 12%, which is not significant. The reason for this is that the increase in bearing capacity is more affected by the properties of the geocell and is less dependent on the properties of the wall. Therefore, the change in the slope of the wall has little effect on the bearing capacity of footing on the geocell-reinforced soil wall.

The effect of the wall slope on the horizontal displacement of the wall is shown in Fig. 14. It confirms that the maximum horizontal displacement of the wall for all ratios s/B occurred at z/H = 0.625 for all slopes of the wall. The results indicate that the decrease in the slope of wall significantly reduces the horizontal displacement of the wall. At the D/H = 0.2, with decreasing the wall slope from 90° to 70° the maximum horizontal displacement of the wall decreases by 62%, 50%, 37% and 32% for footing pressure 50 kPa, 100 kPa, 150 kPa and 200 kPa, respectively. Furthermore, at the D/H = 0.35 and 0.5, the average amount of reduction in the maximum horizontal displacement of the wall was 41% and 38% with decreasing wall slope from 90° to 70°, respectively.

Due to the similarity of the wall behavior at different slopes, the effect of oil pollution on the wall behavior with a 70-degree slope has been evaluated. The results show that by adding 3%, 6%, 9% and 12% oil, the bearing capacity of footing is reduced by an average of 19%, 37%, 45% and 49%, respectively. Also, at footing pressure equal to 100 kPa, the maximum horizontal displacement of the wall increases by 32%, 115%, 159% and 196% for the percentage of pollution 3%, 6%, 9% and 12%, respectively.

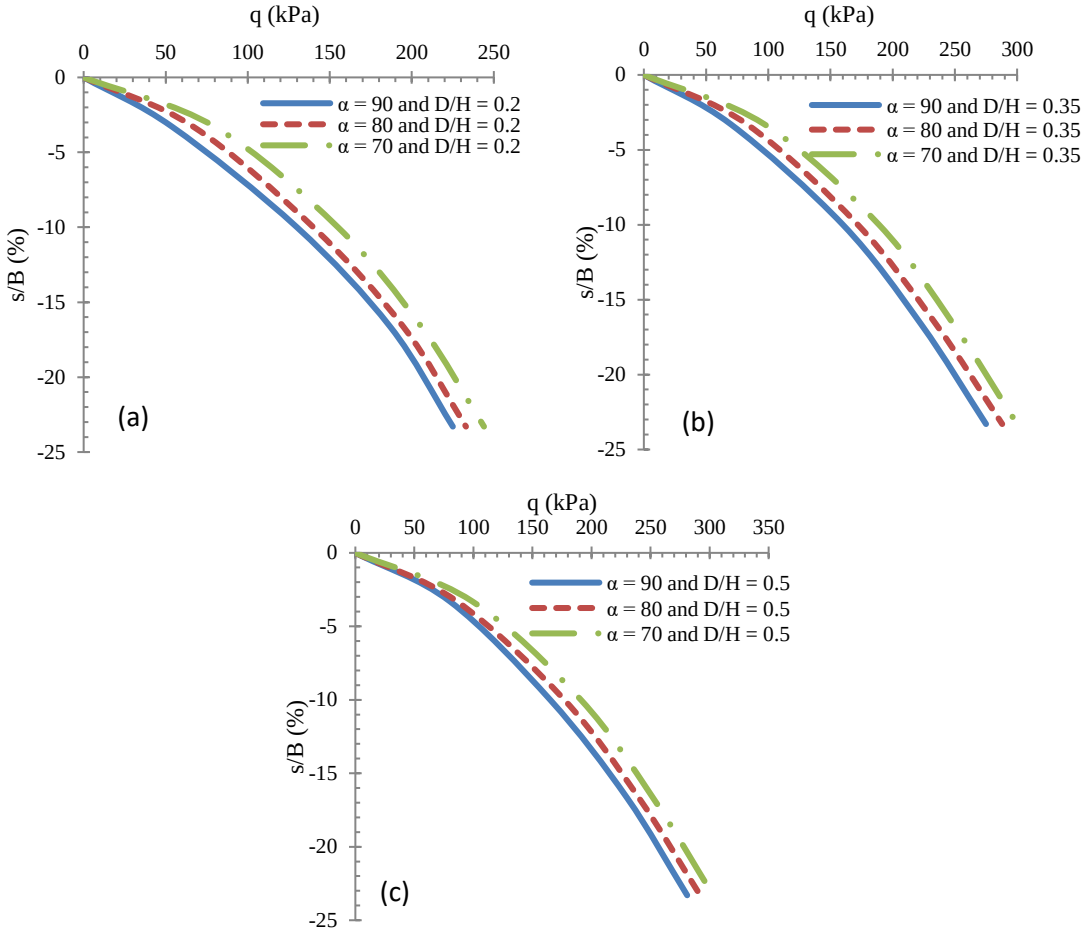

Fig. 13. Bearing capacity (q) - settlement ratio (s/B) curves of the footing on reinforced soil wall for different slope of wall: (a) D/H = 0.2, (b) D/H = 0.35, (c) D/H = 0.5

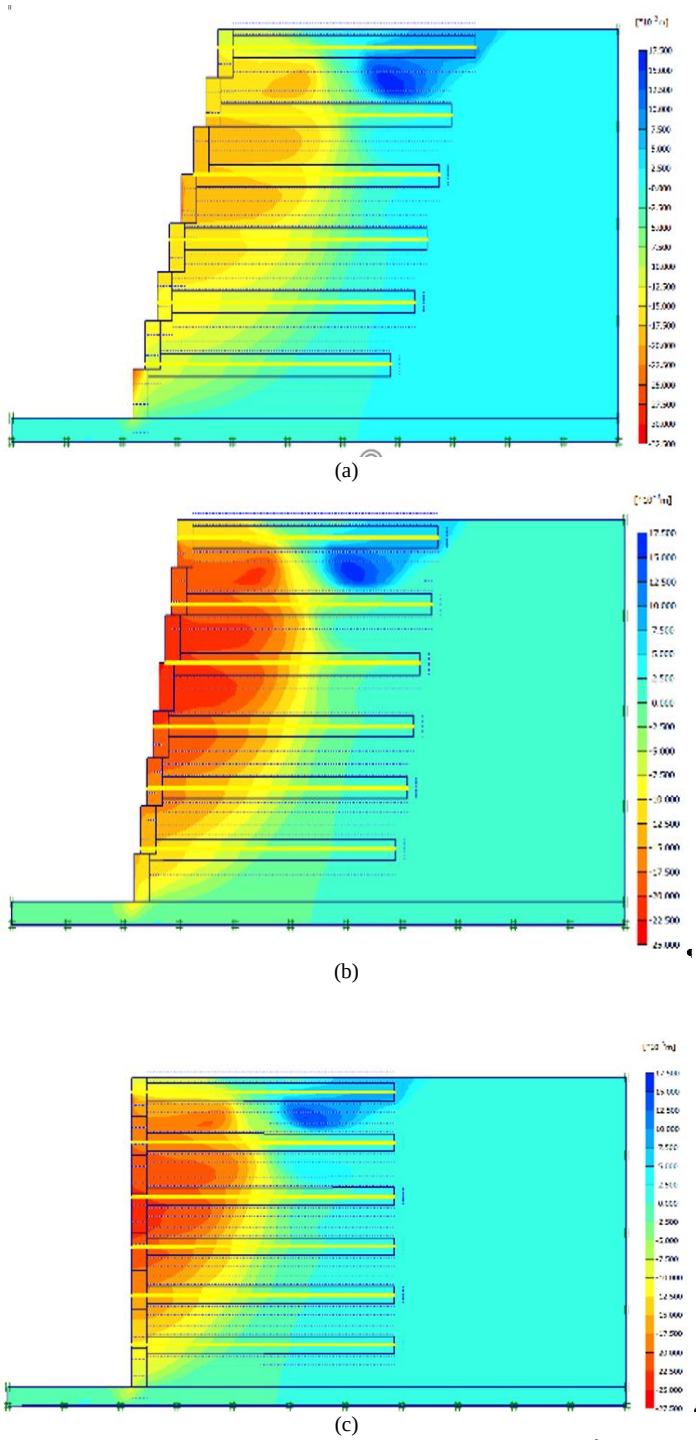

(a)

(b)

(c)

Fig. 14. Horizontal displacement of wall for different wall slope: (a) α = 70˚, (b) α = 80˚, (c) α = 90˚

6. Discussions

The bearing capacity of the footing adjacent to the wall depends on the backfill soil stiffness and the distance between the footing and the wall. Increasing the length and height of geocell means that more soil particles are enclosed by the geocell cells. On the other hand, an increase in the confinement leads to an increase in the soil stiffness and consequently the bearing capacity of the soil. It should be noted that the length of the geocell layer was effective on the stiffness of backfill soil when the required geocell layer length was taken into account, which was equal to 2.16 times the foundation width on each side of the footing center. The change in the value of geocell height (hg) and the pocket size of the geocell (dg) leads to change in the confinement effect, leading to a change in the bearing capacity of the soil. At ratio hg/dg > 2, the cell integrity is reduced and cannot function as a single cell, leading to a reduction in the confinement effect. For this reason, the trend of increasing the bearing capacity of soil decreases in ratios hg/B > 0.6. With an increase in the D/H ratio, the effect of overload due to loading on the wall decreases. Reduction in the effect of overload results in a decrease in ΔH, causing improvement in the load-carrying capacity of the foundation. The results showed that the increase in the footing pressure led to a reduction in the trend of increasing ΔHmax. This can be explained by two main reasons. The essential reason is related to the frictional resistance so that increasing the footing pressure contributes to an increase in the normal stress applied to the geocell layer, promoting higher friction between the geocell layer and the soil. Hence, pulling out the layer became more difficult and ΔHmax diminished. The next reason can be related to the wall facing displacement towards backfill soil by the geocell layer so that with the increase in the footing settlement, the soil particles and subsequently the geocell layer were pulled down; thus, the wall facing by the geocell layer moves towards the soil and ΔHmax drops.

Mixing oil with sand reduces the shear parameters of sand such as the cohesion and the internal friction angle. Although the cohesion of sand is negligible and the effect of oil can be ignored on the cohesion of sand, however, according to Eq. (6), the amount of apparent cohesion decreases with decreasing the angle of internal friction of the sand. Covering the surface of soil particles with oil film reduces the interlock between sand particles, leading to a reduction in the angle of internal friction of sand. Besides, due to lubrication decreases the friction between the cell wall and the soil particles due to lubrication, leading to reduction in the frictional strength. Since the frictional resistance plays an important role in the wall behavior, reducing the frictional resistance weakens the wall performance. One of the negative effects of the oil pollution is the reduction in the safety factor of the wall. To evaluate the safety factor of the wall against sliding, the horizontal pressure of the backfill soil and the horizontal pressure of the foundation must be calculated. The horizontal pressure of the backfill soil can be calculated by Rankin's theory (1857) according to Eq .(9):

$$\sigma_{az} = \gamma z \, tan^2\left(45 - \frac{\varphi}{2}\right) - 2c \tan(45 - \frac{\varphi}{2}) \qquad (9)$$

where γ = the dry unit weights of soil, z = the wall height from above and φ = the internal friction angle of soil, which is equal to 34 degrees. Also, the horizontal pressure of the foundation can be calculated by Laba and Kennedy (1986) according to Eq (10):

$$\sigma_{az} = [\frac{2q}{\pi}(\beta - \sin\beta \times \cos 2\alpha)] \qquad (10)$$

where q = the footing pressure, β and α are shown in Fig. 15 and D = the horizontal distance of the foundation from the wall is equal to 0.35. The safety coefficient of the sliding usually taken as 1.5 (Eq. 11):

$$FS_S = \frac{\sum F_R}{\sum F_a} \geq 1.5 \quad (11)$$

where F_R = the resistant force (v1) and F_a = the active force (F_a1 and F_a2).

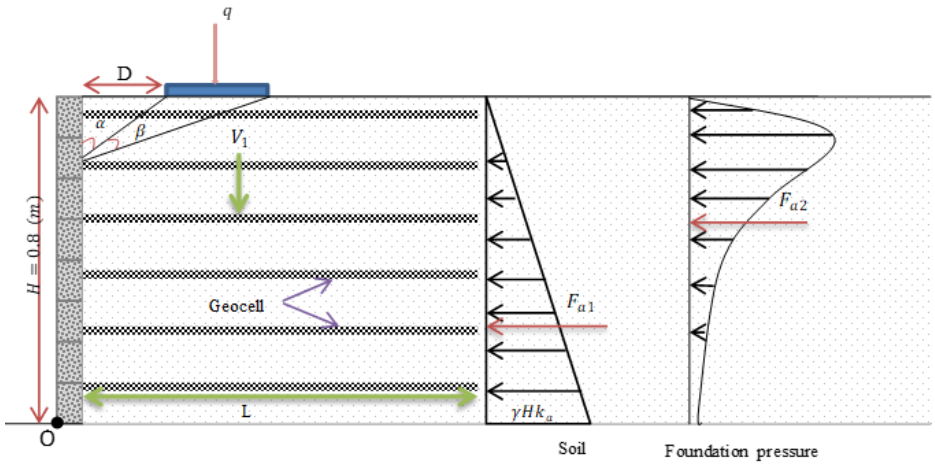

Fig. 15. Forces applied to the geocell-reinforced soil wall

Table 9 shows the safety factor of the wall against sliding for different the amount of oil and the footing pressure. It can be seen in Table 9 that with increasing the amount of oil decrease the safety factor of the wall against sliding. The reason for this phenomenon is that the frictional resistance decreases with increasing weaving amount of oil.

Table 9 safety factor of the wall against sliding for D/H = 0.35 and L/H = 1.0

	Safety factor				
Footing pressure (kPa)	***Amount of oil (%)***				
	0	*3*	*6*	*9*	*12*
0	*4.82*	*4*	*3.46*	*3*	*2.83*
50	*1.43*	*1.32*	*1.2*	*1.12*	*1.06*
100	*1.13*	*1.05*	*0.96*	*0.89*	*0.85*
150	*1.02*	*0.94*	*0.86*	*0.81*	*0.77*

7. Conclusions

In this paper, the behavior of abutment wall reinforced with geocell material under conditions with and without oil contamination was evaluated by numerical modeling. In this research study, the advantages of geocell material as well as the disadvantages of oil contamination were investigated by evaluating the pressure-settlement behavior of strip footing and ΔHmax. The variable parameters of this study included the L/H ratio, the D/H ratio, the hg/B ratio, the number of geocell layers, the wall slop and the percentage of oil. The following conclusions can be drawn:

- Increasing L/H and D/H ratios lead to an increase in the bearing capacity of footing and decrease in the horizontal displacement of the wall. As for different values of the D/H ratio, it can be said that the optimum geocell length is equal to 1.0 times the wall height. The oil contamination has a negative effect on the wall performance.

- Although increasing the geocell height increases the bearing capacity and reduces the horizontal displacement of the wall, but, the backfill soil contamination due to oil leads to a reduction in the positive effect of the geocell height.
- The increase in the number of geocell layers leads to an increase in the soil stiffness, leading to increase in the bearing capacity of the footing. With a 33% increase in the number of geocell layers, the bearing capacity of the footing can be increased by up to 50%. Also, the negative effect of oil contamination on the horizontal displacement of the wall can be decreased by increasing the number of geocell layer
- As the slope of the wall decreases, the bearing capacity of the footing increases and the horizontal displacement of the wall decreases. However, the wall slope has no effect on the location of the maximum horizontal displacement of the wall. Increasing the percentage of soil contamination due to oil significantly increases the horizontal displacement of the wall.

8. References

Abdelhalim, R.A., El Sawwaf, M., Nasr, A.M., Farouk, A. 2020. Experimental and numerical studies of laterally loaded piles located near oil-contaminated sand slope. Engineering Science and Technology, 23, 744–757. https://doi.org/10.1016/j.jestch.2020.03.001.

Ahmadi, M., Ebadi, T., Maknoon, R. 2021. Effects of crude oil contamination on geotechnical properties of sand-kaolinite mixtures. Engineering Geology, 283, 106021. https://doi.org/10.1016/j.enggeo.2021.106021.

Al-Adili, A., Alsoudany, K.Y., Shakir, A. 2017. Investigation of crude oil pollution effect on stiffness characteristic of sandy and gypseous soil. Soil Mechanics and Foundation Engineering, 54(4), 276-282. http://doi.org/10.1007/s11204-017-9469-x.

Alfach, M.T., Wilkinson, S. 2020. Effect of crude-oil-contaminated soil on the geotechnical behaviour of piles foundation. Geotechnical Research, 7(2), 76–89. https://doi.org/10.1680/jgere.19.00017.

Bathurst, R.J., Karpurapu, R.G. 1993. Large-scale triaxial compression testing of geocell-reinforced granular soils. Geotechnical Testing Journal, 16, 296–303. http://doi.org/10.1520/GTJ10050J.

Biabani, M.M., Indraratna, B., Trung Ngo, N. 2016. Modelling of geocell-reinforced subballast subjected to cyclic loading. Geotextiles and Geomembranes, 44, 489-503. http://doi.org/10.1016/j.geotexmem.2016.02.001.

Changizi, F., A. Razmkhah., H. Ghasemzadeh., and M. Amelsakhi. 2022. Behavior of geocell-reinforced soil abutment wall: A physical modeling. Journal of Materials in Civil Engineering, 34(3), 04021495. https://doi.org/10.1061/(ASCE)MT.1943-5533.0004132.

Chen, R.H., Chiu, Y.M. 2008. Model tests of geocell retaining structures. Geotextiles and Geomembranes, 26, 56–70.: https://doi.org/10.1016/j.geotexmem.2007.03.001.

Chen, R.H., Wu, C.P., Huang, F.Ch., Shen, Ch.W. 2013. Numerical analysis of geocell-reinforced retaining structures. Geotextiles and Geomembranes, 39, 51-62. http://doi.org/10.1016/j.geotexmem.2013.07.003.

Dash, S.K. 2010. Influence of Relative Density of Soil on Performance of Geocell-Reinforced Sand Foundations. Journal of Materials in Civil Engineering, 22, 533-538. http://doi.org/10.1061/(ASCE)MT.1943-5533.0000040.

Dash, S.K. 2012. Effect of geocell type on load-carrying mechanisms of geocell-reinforced sand foundations. International Journal of Geomechanics, 12, 537-548. https://doi.org/10.1061/(ASCE)GM.1943-5622.0000162.

Fadhil Al-Adly, A.I., Fadhil, A.M., Fattah, M.Y. 2019. Bearing capacity of isolated square footing resting on contaminated sandy soil with crude oil. Egyptian Journal of Petroleum, 28, 281–288. https://doi.org/10.1016/j.ejpe.2019.06.005.

Ghasemzadeh, H., Tabaiyan, M. 2017. The Effect of Diesel Fuel Pollution on the Efficiency of Soil stabilization Method. Geotechnical and Geological Engineering, 35, 475–484. https://doi.org/10.1007/s10706-016-0121-8.

Hegde, A., Sitharam, T.G. 2013. Experimental and numerical studies on footings supported on geocell reinforced sand and clay beds. International Journal of Geotechnical Engineering, 7(4), 346–354. https://doi.org/10.1179/1938636213Z.00000000043.

Hegde, A.M, Sitharam, T.G. 2015. Three-dimensional numerical analysis of geocell-reinforced soft clay beds by considering the actual geometry of geocell pockets. Canadian Geotechnical Journal, 52, 1–12. https://doi.org/10.1139/cgj-2014-0387.

Inti, S., Tandon, V. 2021. Design of geocell reinforced roads through fragility modeling. Geotextiles and Geomembranes, 49(5), 1085-1094. https://doi.org/10.1016/j.geotexmem.2021.03.003.

Kermani, M., Ebadi, T. 2012. The effect of oil contamination on the geotechnical properties of fine-grained soils. Soil Sediment Contam, 21(5), 655–671. https://doi.org/10.1080/15320383.2012.672486.

Khosravi, E., Ghasemzadeh, H., Sabour, M.R., Yazdani, H. 2013. Geotechnical properties of gas oil-contaminated kaolinite. Engineering Geology, 166, 11–16. https://doi.org/10.1016/j.enggeo.2013.08.004.

Laba, J.T., Kennedy, J.B. 1986. Reinforced earth retaining wall analysis and design. Can. Geotech. J. 23(3), 317 – 326. https://doi.org/10.1139/t86-045.

Li, L. H., Yu. C.D., Xiao. H.L., Feng. Q.W., Ma. Q., Yin, J.H. 2020. Experimental study on the reinforced fly ash and sand retaining wall under static load. Construction and Building Materials, 248, 118678. https://doi.org/10.1016/j.conbuildmat.2020.118678.

Leshchinsky, D., Ling, H.I., Wang, J.P., Rosen, A., Mohri, Y. 2009. Equivalent seismic coefficient in geocell retention systems. Geotextiles and Geomembranes 27, 9–18. https://doi.org/10.1016/j.geotexmem.2008.03.001.

Ling, H.I., Leshchinsky, D., Wang, J.P., Mohri, Y., Rosen, A. 2009. Seismic Response of Geocell Retaining Walls: Experimental Studies. Journal of Geotechnical and Geoenvironmental Engineering, 135, 515-524. https://doi.org/10.1061/(ASCE)1090-0241(2009)135:4.(۵۱۵)

Madhavi Latha, M., Rajagopal, K. 2007. Parametric finite element analyses of geocell-supported embankments. Canadian Geotechnical Journal, 44, 917–927. https://doi.org/10.1139/T07-039.

Madhavi Latha, M., Somwanshi, A. 2009. Effect of reinforcement form on the bearing capacity of square footings on sand. Geotextiles and Geomembranes, 27, 409–422. https://doi.org/10.1016/j.geotexmem.2009.03.005.

Madhavi Latha, G., Manju, G.S. 2016. Seismic response of geocell retaining walls through shaking table tests. International Journal of Geosynthetics and Ground Engineering, 2, 7. https://doi.org/10.1007/s40891-016-0048-4.

Mehdipour, I., Ghazavi, M., Moayed, R.Z. 2013. Numerical study on stability analysis of geocell reinforced slopes by considering the bending effect. Geotextiles and Geomembranes, 37, 23–34. https://doi.org/10.1016/j.geotexmem.2013.01.001.

Moghaddas Tafreshi, S.N., Dawson, A.R. 2010. Comparison of bearing capacity of a strip footing on sand with geocell and with planar forms of geotextile reinforcement. Geotextiles and Geomembranes, 28, 72–84. https://doi.org/10.1016/j.geotexmem.2009.09.003.

Moghaddas Tafreshi, S.N., Khalaj, O., Dawson, A.R. 2014. Repeated loading of soil containing granulated rubber and multiple geocell layers. Geotextiles and Geomembranes, 42, 25-38. http://doi.org/10.1016/j.geotexmem.2013.12.003.

MoghaddasTafreshi, S.N., Sharifi, P., Dawson, A.R. 2016. Performance of circular footings on sand by use of multiple-geocell or –planar geotextile reinforcing layers. Soils and Foundations, 56(6), 984–997: http://doi.org/10.1016/j.sandf.2016.11.004.

Nasehi, S.A., Uromeihy, A., Nikudel, M.R., Morsali, A. 2015. Influence of gas oil contamination on geotechnical properties of fine and coarse-grained soils. Geotechnical and Geological Engineering, 34(1), 333–345. http://doi.org/10.1007/s10706-015-9948-7.

Nasr, A.M.A. 2009. Experimental and Theoretical Studies for the Behavior of Strip Footing on Oil-Contaminated Sand. Journal of Geotechnical and Geoenvironmental Engineering, 135(12), 1814-1822. http://doi.org/10.1061/ASCEGT.1943-5606.0000165.

Pokharel, S.K., Han, J., Leshchinsky, D., Parsons, R.L., Halahmi, I. 2010. Investigation of factors influencing behavior of single geocell-reinforced bases under static loading. Geotextiles and Geomembranes 28, 570-578. http://doi.org/10.1016/j.geotexmem.2010.06.002.

Pokharel, S.K., Han, J., Leshchinsky, D., Parsons, R.L. 2018. Experimental evaluation of geocell-reinforced bases under repeated loading. International Journal of Pavement Research and Technology, 11(2), 114-127. https://doi.org/10.1016/j.ijprt.2017.03.007.

Rajagopal, K., Krishnaswamy, N.R., and Madhavi Latha, G. 1999. Behavior of sand confined in single and multiple geocells. Geotextiles and Geomembranes, 17, 171–184. https://doi.org/10.1016/S02661144(98)00034-X.

Rankine, W. M. J. 1857. On Stability on Loose Earth," Philosophic Transactions of Royal Society, London, Part I, 9–27.

Safehiana, H., Rajabi, A.M., Ghasemzadeh, H. 2018. Effect of diesel-contamination on geotechnical properties of illite soil. Engineering Geology, 241, 55–63. https://doi.org/10.1016/j.enggeo.2018.04.020.

Singh, S.K., Srivastava, R.K., Siby, J. 2008. Settlement characteristics of clayey soils contaminated with petroleum hydrocarbons. Soil and Sediment Contamination: An International Journal, 17(3), 290–300. https://doi.org/10.1080/15320380802007028.

Skinner, G.D., R. K. Rowe. 2005. Design and behaviour of a geosynthetic reinforced retaining wall and bridge abutment on a yielding foundation. Geotextiles and Geomembranes, 23, 234–60. https://doi.org/10.1016/j.geotexmem.2004.10.001.

Soltani-Jigheh, H., Vafaei Molamahmood, H., Ebadi, T., Soorki, A.A. 2018. Effect of Oil-Degrading Bacteria on Geotechnical Properties of Crude Oil–Contaminated Sand. Environmental & Engineering Geoscience, 24 (3), 333–341. https://doi.org/10.2113/EEG-1883.

Song, F., Xie, Y.L., Yang, Y.F., Yang, X.H. 2014. Analysis of failure of flexible geocell-reinforced retaining walls in the centrifuge. Geosynthetics International, 21(6), 342-351. http://doi.org/10.1680/gein.14.00022.

Song, F. Liu, H., Hu, H., Xie, Y. 2018a. Centrifuge Tests of Geocell-Reinforced Retaining Walls at Limit Equilibrium. Journal of Geotechnical and Geoenvironmental Engineering, 144(3), 04018005. http://doi.org/10.1061/(ASCE)GT.1943-5606.0001849.

Song, F., i Liu, H., Ma, L., Hu, H. 2018b. Numerical analysis of geocell-reinforced retaining wall failure modes. Geotextiles and Geomembranes, 46, 284–296. https://doi.org/10.1016/j.geotexmem.2018.01.004.

Soudé, M., Chevalier, B., Grédiac, M., Talon, A., Gourvès, R. Experimental and numerical investigation of the response of geocell-reinforced walls to horizontal localized impact. Geotextiles and Geomembranes, 39, 39-50. http://doi.org/10.1016/j.geotexmem.2013.07.006.

Tatsuoka, F., Tateyama, M. Koda, K. Kojima, T. Yonezawa, Y. Shindo, S. Tamai, Sh. 2016. Research and construction of geosynthetic-reinforced soil integral bridges. Transportation Geotechnics, 8, 4–25. https://doi.org/10.1016/j.trgeo.2016.03.006.

Thallak, S.G., Saride, S., Dash, S.K. 2007. Performance of surface footing on geocell-reinforced soft clay beds. Geotechnical and Geological Engineering, 25, 509–524. https://doi.org/10.1007/s10706-007-9125-8.

Venkateswarlu, H., Ujjawal, K.N., Hegde, A. 2018. Laboratory and numerical investigation of machine foundations reinforced with geogrids and geocells. Geotextiles and Geomembranes, 46(6), 882-896. https://doi.org/10.1016/j.geotexmem.2018.08.006.

Xiao, Ch., Han, J., Zhang, Z. 2016. Experimental study on performance of geosynthetic-reinforced soil model walls on rigid foundations subjected to static footing loading. Geotextiles and Geomembranes, 44, 81-94. https://doi.org/10.1016/j.geotexmem.2015.06.001.

Xie, Y., Yang, X. 2009. Characteristics of a new-type geocell flexible retaining wall. Journal of Materials in Civil Engineering, 21(4), 171-175. https://doi.org/10.1061/(ASCE)0899-1561(2009)21:4(171).

Yang, X., Han, J., Pokharel, S.K., Manandhar, Ch., Parsons, R.L., Leshchinsky, D., Halahmi, I. 2012. Accelerated pavement testing of unpaved roads with geocell-reinforced sand bases. Geotextiles and Geomembranes, 32, 95-103. https://doi.org/10.1016/j.geotexmem.2011.10.004.

Zhou, H., Wen, X. 2008. Model studies on geogrid- or geocell-reinforced sand cushion on soft soil. Geotextiles and Geomembranes, 26, 231–238. https://doi.org/10.1016/j.geotexmem.2007.10.002.